International Journal of Nanomedicine

Dovepress
open access to scientific and medical research

Open Access Full Text Article

ORIGINAL RESEARCH

# Functional Peptide-Loaded Gelatin Nanoparticles as Eyedrops for Cornea Neovascularization Treatment

Ya-Chun Chu[1,2,*], Hsu-Wei Fang[2,3,*], Yu-Yi Wu[1], Yu-Jun Tang[1], Erh-Hsuan Hsieh[1], YiZhou She[4], Che-Yi Chang[1], I-Chan Lin[5,6], Yin-Ju Chen[1,7–9], Guei-Sheung Liu[1,10–12], Ching-Li Tseng[1,8,9,13]

[1]Graduate Institute of Biomedical Materials and Tissue Engineering, College of Biomedical Engineering, Taipei Medical University, Taipei City, Taiwan; [2]Department of Chemical Engineering and Biotechnology, National Taipei University of Technology, Taipei City, Taiwan; [3]Institute of Biomedical Engineering and Nanomedicine, National Health Research Institutes, Miaoli County, Taiwan; [4]School of Biomedical Engineering, College of Biomedical Engineering, Taipei Medical University, Taipei City, Taiwan; [5]Department of Ophthalmology, Wan Fang Hospital, Taipei Medical University, Taipei City, Taiwan; [6]Department of Ophthalmology, School of Medicine, College of Medicine, Taipei Medical University, Taipei City, Taiwan; [7]Department of Radiation Oncology, Taipei Medical University Hospital, Taipei City, Taiwan; [8]International Ph.D. Program in Biomedical Engineering, College of Biomedical Engineering, Taipei Medical University, Taipei City, Taiwan; [9]Center for Precision Medicine and Translational Cancer Research, Taipei Medical University Hospital, Taipei City, Taiwan; [10]Centre for Eye Research Australia, Royal Victorian Eye and Ear Hospital, East Melbourne, VIC, Australia; [11]Ophthalmology, Department of Surgery, University of Melbourne, East Melbourne, VIC, Australia; [12]Menzies Institute for Medical Research, University of Tasmania, Hobart, TAS, Australia; [13]Research Center of Biomedical Device, College of Biomedical Engineering, Taipei Medical University, Taipei City, Taiwan

*These authors contributed equally to this work

Correspondence: Ching-Li Tseng, Tel +886 2 2736 1661 (ext. 5214), Email chingli@tmu.edu.tw



**Background:** Corneal neovascularization (NV) is a process of abnormal vessel growth into the transparent cornea from the limbus and can disturb the light passing through the cornea, resulting in vision loss or even blindness. The use of nanomedicine as an effective therapeutic formulation in ophthalmology has led to higher drug bioavailability and a slow drug release rate. In this research, we designed and explored the feasibility of a new nanomedicine, gp91 ds-tat (gp91) peptide-encapsulated gelatin nanoparticles (GNP-gp91), for inhibiting corneal angiogenesis.

**Methods:** GNP-gp91 were prepared by a two-step desolvation method. The characterization and cytocompatibility of GNP-gp91 were analyzed. The inhibition effect of GNP-gp91 on HUVEC cell migration and tube formation was observed by an inverted microscope. The drug retention test in mouse cornea was observed by in vivo imaging system, fluorescence microscope, and DAPI/TAMRA staining. Finally, the therapeutic efficacy and evaluation of neovascularization-related factors were conducted through the in vivo corneal NV mice model via topical delivery.

**Results:** The prepared GNP-gp91 had a nano-scale diameter (550.6 nm) with positive charge (21.7 mV) slow-release behavior (25%, 240hr). In vitro test revealed that GNP-gp91 enhanced the inhibition of cell migration and tube formation capacity via higher internalization of HUVEC. Topical administration (eyedrops) of the GNP-gp91 significantly prolongs the retention time (46%, 20 min) in the mouse cornea. In chemically burned corneal neovascularization models, corneal vessel area with a significant reduction in GNP-gp91 group (7.89%) was revealed when compared with PBS (33.99%) and gp91 (19.67%) treated groups via every two days dosing. Moreover, GNP-gp91 significantly reduced the concentration of Nox2, VEGF and MMP9 in NV's cornea.

**Conclusion:** The nanomedicine, GNP-gp91, was successfully synthesized for ophthalmological application. These data suggest that GNP-gp91 contained eyedrops that not only have a longer retention time on the cornea but also can treat mice corneal NV effectively delivered in a low dosing frequency, GNP-gp91 eyedrops provides an alternative strategy for clinical ocular disease treatment in the culture.

**Keywords:** gp91 peptide, gelatin, nanoparticles, ocular retention, control release, corneal neovascularization, eye drops

Received: 23 November 2022
Accepted: 7 March 2023
Published: 23 March 2023

**Graphical Abstract**

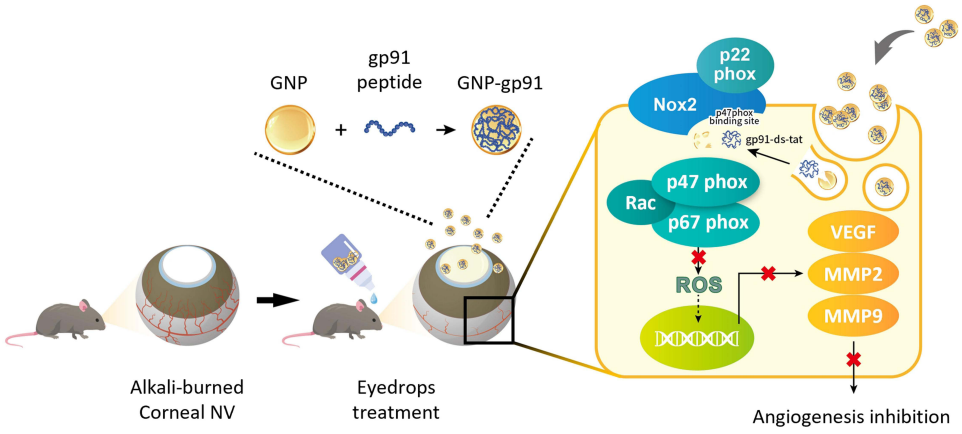


## Introduction

Corneal neovascularization (NV) is a pathological condition of the cornea characterized by the invasion of new blood vessels into the avascular corneal regions from the limbus.[1] Common causes of corneal neovascularization include chemical burns, trauma, contact lens wear, hypoxia, infection, corneal graft rejection, and immunological disease.[1] The increased permeability of these new vessels leads to chronic corneal edema, lipid exudation, inflammation, and scar formation.[2–4] The mechanism underlying inflammation-induced NV results from the disruption of angiogenic and antiangiogenic balance in the cornea, which leads to significant corneal transparency change and visual impairment.[3,5,6] Several medical and surgical options have been used to treat corneal NV, such as laser ablation, photodynamic therapy, and anti-vascular endothelial growth factor (VEGF) treatment.[3,7] Anti-VEGF treatment administered by topical, subconjunctival, and intraocular application is one of the major therapeutics used for ocular neovascularization treatment nowadays.[3,7]

While anti-VEGF treatment is promising, partial efficacy, delivered in an invasive manner, resistance for longer treatment, and side effects have limited its clinical effect. In addition to VEGF signaling, there are several other angiogenic factors are also known to be involved in ocular neovascularization.[8–10] Thus, new compounds/drugs or formulas have also been developed for application in inhibiting vessel formation to effectively treat ocular NV. For instance, blockade of nicotinamide adenine dinucleotide phosphate (NADPH) oxidases, especially NADPH oxidase 2 (Nox2), by gp91ds-tat peptide prevents diabetes-induced premature retinal endothelial cell senescence.[11] Previous studies demonstrated that gp91ds-tat peptide (gp91) can mediate oxidative stress and reduce reactive oxygen species (ROS),[12,13] which mediates many biological responses, including angiogenesis.[14] Therefore, gp91 is considered a candidate for anti-angiogenic therapy.

For drug delivery to the eye, subconjunctival injection and topical therapy are the two feasible approaches.[15,16] Compared with subconjunctival injection, topical therapy is the preferred method for patients because of the relatively safe and widely applicable approach. However, a low bioavailability (<5%) of topical delivery due to various anatomical and physiological barriers, such as not allowing therapeutic agents to penetrate the corneal epithelium due to intracellular tight junctions,[17,18] and constraints such as blinking and lacrimal draining have limited its applications.[18,19] Higher concentrations or repeated dosing is a way to overcome these limitations of drug administration, but these methods are not accurate due to a dramatic variation in the therapeutic concentration in the ocular tissue.[19–21] These limitations have prompted researchers to develop new and effective drug delivery systems for eye treatment.

Nanoparticles (NPs) are distinct particulate systems with a size of 10–1000 nm and a specific surface charge.[19] With a size lower than 1000 nm, not only the scratching and irritation of the eyes can be avoided when using

nanoparticles,[22,23] but the corneal permeability of drugs will also be enhanced.[24,25] Variant kinds of nanoparticles such as liposome, gold nanoparticles, and polymeric nanoparticles were studied.[1,19,24] The biological polymer, gelatin, was chosen in the study as the particle matrix because of its biocompatibility and biodegradation.[26,27] Gelatin nanoparticles (GNPs) can be fabricated with different surface charge (manipulated by different types of gelatins), and the drug release behavior of GNP can be controlled by changing the crosslinking agent and time.[27] Owing to the cornea/conjunctiva having a negatively charged ocular surface, cationic NPs can be attracted to the ocular surface for topical drug delivery,[26,28,29] and the corneal permeability of drug-loaded cationic GNP will also increase due to electrostatic interaction.[26,29,30] Furthermore, GNPs were successful in enhancing drug retention on the ocular surface and can be applied as eye drops for treating corneal disease.[25,26,29,30]

In this study, we used gp91 as the active component for treating pathological angiogenesis in cornea. The nanomedicine, gp91-loaded GNP (GNP-gp91) was designed, synthesized, and proceeded properties' examination. The therapeutic efficacy of GNP-gp91 for the inhibition of vessel function was evaluated in vitro and in vivo. The schematic drawing of this study is revealed in Figure 1.

# Materials and Methods

## Materials

Human umbilical vein endothelial cells (HUVECs) were purchased from the Bioresource Collection and Research Center (Hsinchu, Taiwan). Medium 199 and penicillin-streptomycin-neomycin (PSN) antibiotic mixture were purchased from Life Technologies (Camarillo, CA, USA). Fetal bovine serum (FBS) was obtained from HyClone (South Logan, Utah, USA). The endothelial cell growth supplement (ECGS) was bought from Merck Millipore (Billerica, MA, USA). The gp91-ds-tat peptide (gp91) (RKKRRQRRRCSTRIRRQL) and fluorescein isothiocyanate (FITC)-labeled gp91-ds-tat ($gp91^{FITC}$) were synthesized by MDBio Inc. (Taipei, Taiwan). Gelatin type B (derived from bovine skin, Bloom 225), heparin, Triton™ X-100, 4',6-diamidino-2-phenylindole (DAPI), cell counting Kit-8 (CCK-8), live/dead cell double staining kit, lipopolysaccharide (LPS), and 2'7'-dichlorofluorescin diacetate (DCFH-DA) were purchased from Sigma-Aldrich (St. Louis, MO, USA). The Vivaspin 500 ultrafiltration device was purchased from Sartorius (Göttingen, Germany). Float-A-Lyzer®G2 Dialysis Device (MWCO 20 kDa) was acquired from Spectrum Laboratories, Inc. (Rancho Dominguez, CA, USA). Tetramethyl rhodamine succinyl ester (TAMRA-SE) was purchased from Invitrogen

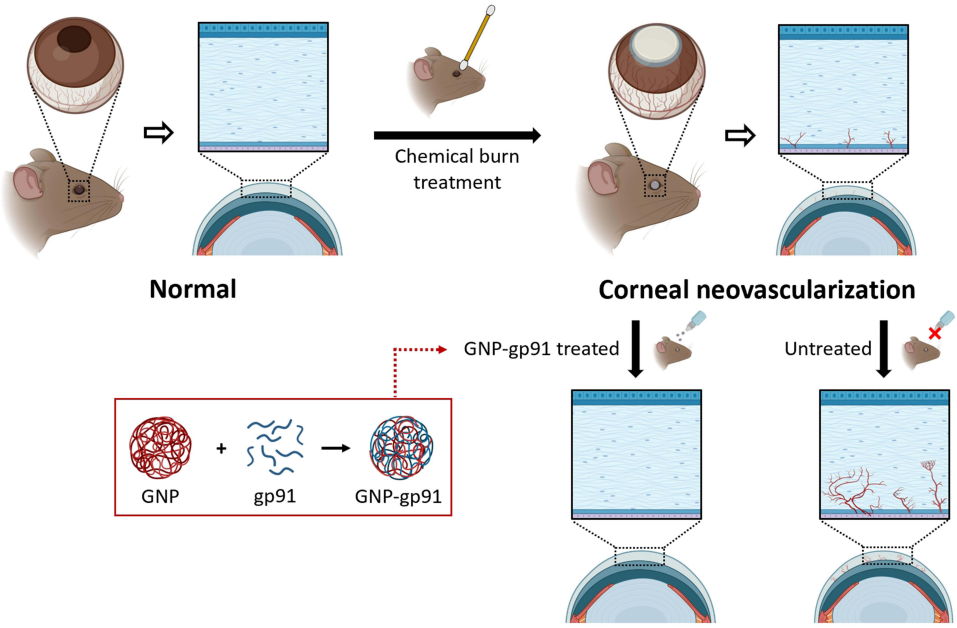


**Figure 1** Schematic illustration of gp91ds-tat peptide (gp91)-loaded gelatin nanoparticles (GNP-gp91) as eye drops to treat alkali-burned induced corneal neovascularization (NV) in a mouse model.

(Carlsbad, CA, USA). The Matrigel™ matrix was purchased from Corning (Corning, NY, USA). Rompun solution (2%) was obtained from Bayer Korea, Ltd. (Ansan City, Gyeonggi-do, Korea), and Zoletil 50 was purchased from Virbac Animal Health (Vauvert, Nice, France). Topical anesthesia solution (Alcaine® 0.5% ophthalmic solution) was obtained from Alcon-Couvreur N.V. (Puurs, Belgium). Grafco® silver nitrate applicators were purchased from Medline Industries Inc. (Mun-delein, IL, USA). All other chemicals were purchased from Sigma-Aldrich.

## Preparation of GNP and gp91-Loaded GNP (GNP-gp91)

The GNP and GNP-gp91 were prepared by a two-step desolvation method with slightly modified.[30,31] First, 5% (w/v) type B gelatin solution was purified using acetone for the first desolvation to remove gelatin with low molecular weight.[31,32] The residual gelatin was then redissolved in hot water to get gelatin solution (1% w/v) again and adjusted its pH value to 8 or 9 after cooling. Then, 300 μL of deionized water or gp91 peptide solution (gp91) (10 mg/mL) was added into 1 mL gelatin solution separately for preparation of GNP or peptide loaded GNP (GNP-gp91). After that, 1.6 mL ethanol was then added dropwise to the gelatin solution to form gelatin nanoparticles (GNPs); followed by adding 16.25 μL glutaraldehyde (8% (w/v)) and stirring for 30 minutes for crosslinking reaction.[30] Finally, the ethanol was evaporated using a rotary evaporator (EYELA, Tokyo, Japan), and the excess impurities were removed using an ultrafiltration device (Vivaspin 500, MWCO 30 kDa). The GNP and GNP-gp91 were stored at 4 °C in deionized water for further application.

## Characterization of GNP and GNP-gp91

The particle size distribution and zeta potential were analyzed using a zetasizer (Nano ZS 90, Malvern Instruments, Malvern, UK, scattering light: 90°, equilibration time: 180s, temperature: 25°C). The particle morphology was observed using a transmission electron microscope (TEM, Hitachi HT-7700, Tokyo, Japan, acceleration voltage: 75.0 kV). Samples were dropped on carbon-coated nickel mesh and dried overnight before analysis. The quantification of gp91 was determined using the Bicinchoninic Acid (BCA) protein assay to measure the unencapsulated gp91 peptide content after GNP-gp91 preparation, and the encapsulation efficiency (EE) was calculated as the final peptide content compared with the initial added peptide content. For the drug release examination, the content of fluorescent dye (FITC) released out the dialysis bag was quantified for dye/drug release. The FITC labeled gp91 ($gp91^{FITC}$) and $gp91^{FITC}$-loaded GNP ($GNP\text{-}gp91^{FITC}$) were added into a A-Lyzer®G2 Dialysis Device, then soaked in PBS and stirred at a condition of 100 rpm and 37°C. Solutions were sampled at the indicated time and examined using a microplate reader (Varioskan Flash, Thermo Fisher Scientific) at excitation wavelength: 494 nm and emission wavelength: 518 nm. We compared the optical density (OD) value of tested samples with FITC standard curve for dye quantification. The total amount of dye released was calculated as the accumulated release rate for the release evaluation.

## In vitro Study

### Cell Viability

Human umbilical vascular endothelial cells (HUVECs) were used in this study and cultured in M199 medium contained supplemented with 10% fetal bovine serum, 1% penicillin/streptomycin, 30 μg/mL endothelial cell growth supplement, and 25 U/mL heparin. All in vitro experiments were incubated in an incubator at 37°C in a 5% $CO_2$ atmosphere. For cytotoxicity test, HUVECs were seeded in a 96-well plate at a density of $5 \times 10^3$ cells/well and cultured overnight. After removing the cultured medium, HUVECs were co-cultured with various formulations (GNP, gp91, and GNP-gp91) at peptide concentrations of 50–150 μg/mL for 24 hours and 72 hours. After removing the co-cultured medium, 100 μL medium and 10 μL Cell Counting Kit-8 (CCK-8) reagent were mixed and added into each well for 3 hours. Finally, the cell viability was calculated after analyzing the absorbance using a microplate reader (Epoch 2, BioTek, Winooski, VT, USA) at 450 nm. The percentage of viable cells was calculated in comparison to that of the control cells cultured with medium only. For Live&Dead staining, HUVECs were seeded in a 24-well plate at a density of $3.3 \times 10^4$ cells/well and cultured overnight. After removing the cultured medium, HUVECs were co-cultured with various formulations (333 μg/mL GNP, 100 μg/mL gp91, and GNP-gp91: 333 μg/mL GNP with 100 μg/mL gp91) for 1 and 3 days. After removing the co-cultured medium, the diluted calcein-AM and propidium iodide

(PI) were added into each well for 10 min. Finally, the cell morphology was observed using an inverted fluorescence microscope (DMi8, Leica, Wetzlar, Germany).

### Cellular Uptake

HUVECs were seeded in a 24-well plate at a density of $2 \times 10^5$ cells/well and cultured overnight. After removing the cultured medium, HUVECs were co-cultured with $gp91^{FITC}$ and GNP-$gp91^{FITC}$ ($gp91^{FITC}$ concentration: 120 μg/mL) for 0.5 hours and 2 hours. After removing the co-cultured medium, HUVECs were collected by adding 0.05% trypsin-EDTA for 5 minutes, centrifuged, and resuspended in PBS. Finally, the cellular uptake results were analyzed using a flow cytometer (Attune™ NxT Acoustic Focusing Cytometer, Thermo Fisher Scientific, Carlsbad, CA). The auto-fluorescent intensity of cells was adjusted to the range of $10^2$–$10^3$ as the background value.

### Reactive Oxygen Species (ROS) Examination

The ROS content of cells was determined using dichloro-dihydro-fluorescein diacetate (DCFH-DA) assay.[33] Briefly, HUVECs were seeded in a 96-well plate at a density of $5 \times 10^3$ cells/well and cultured overnight. After removing the cultured medium, mediums with 500 ng/mL lipopolysaccharide (LPS) were added and tested for 6 hours. After LPS stimulation, mediums were removed, and HUVECs were then co-cultured with various formulations (333 μg/mL GNP, 100 μg/mL gp91, and GNP-gp91: 333 μg/mL GNP with 100 μg/mL gp91) for 24 hours. After removing the co-cultured medium, 100 μL DCFH-DA reagent (20 μM) was added and incubated for 30 minutes in the dark. The ROS content was determined using a spectral scanning multimode reader (Varioskan Flash, Thermo Scientific, USA, excitation wavelength: 485 nm, emission wavelength: 530 nm).

### Cell Migration

HUVECs were seeded in a 24-well plate with 0.1% gelatin pre-coating at a density of $2 \times 10^5$ cells/well and cultured overnight. A 200 μL tip was used to scrape the cell layer to form a gap between cells and washed with PBS to remove cell fragments or detached cells. HUVECs were then co-cultured with various formulations (medium, GNP, gp91 and GNP-gp91 (at the same peptide concentration; 100 μg/mL)) for 2, 6, and 8 hours. Finally, the cell morphology was captured using an inverted fluorescence microscope (IX81, Olympus, Tokyo, Japan). The wound closure was measured by ImageJ software (http://imagej.nih.gov/ij/; provided in the public domain by the National Institutes of Health, Bethesda, MD, USA). Comparison of cells in gap area with initial gap area (0 h) showing as percentage of wound closure was calculated.

### Endothelial Tube Formation Assay

HUVECs ($1.1x10^4$ cells/well) and various formulations (medium, GNP, gp91 and GNP-gp91 (at the same gp91 concentration; 100 μg/mL)) were mixed and added into a 96-well plate with Matrigel™ pre-coating and cultured for 8 hours. The tube morphology was captured and observed using an inverted fluorescence microscope (IX81, Olympus, Tokyo, Japan).

## In vivo Study

C57BL/6J male mice, aged 8–14 weeks, were used in this study. The experimental procedure was performed according to the ARVO Statement for the Use of Animals in Ophthalmic and Vision Research and approved by the Institutional Animal Care and Use Committee (IACUC) of Taipei Medical University (IACUC approval no. LAC-2016-0404 and LAC-2017-0344). The animals were housed in standard cages in a light-controlled room at 23 ± 2 °C, relative humidity of 60% ± 10%, and alternating 12-hour light-dark cycle. Each animal was provided food and water ad libitum.

### NPs Retention and Distribution on the Ocular Surface

For this test, red fluorescence (TAMRA-SE) was conjugated with GNP/GNP-gp91 for obviously tracking it in vivo, since tissue auto-fluorescence is usually green. The red fluorescent dye (TAMRA-SE) was conjugated with GNP and GNP-gp91 to prepare $GNP^{TAMRA}$ and $GPN\text{-}GP91^{TAMRA}$. A Xenogen in vivo imaging system (IVIS 200) (Alameda, CA, USA) was used to detect the fluorescent signal in the eyes with modified as previous study.[29,30] The mice were anesthetized, and 5 μL eye drops in variant formula ($GNP^{TAMRA}$, TAMRA, and GNP-$gp91^{TAMRA}$ with TAMRA concentration of 37

μg/mL) were directly dropped onto mice eyes. The fluorescence intensity was photographed and quantified using the Living Image software. A comparison of the fluorescence intensity with the initial intensity at different time intervals was revealed in percentage. After this test, the entire eyeball of each mouse was extracted and collected. Whole eyeballs were managed by cryosection process via sectioning in a cryostat microtome (CM 3050S, Leica Microsystems, Wetzlar, Germany). The tissue sections were then stained with DAPI for nuclear labeling and examined under an inverted fluorescence microscope (IX81, Olympus, Tokyo, Japan) to observe nanoparticle distribution in the cornea.

### Evaluation of Corneal Neovascularization Treatment

Seventy-two mice were used in this study for three repeated tests, with six mice in each group (Control, PBS, gp91, and GNP-gp91). The corneal NV mice model was induced as previous study.[34] Briefly, the mice were anesthetized and immobilized before examination. Next, topical administration of Alcaine (Alcon, Puurs, Belgium) for local anesthesia, followed by pressing the tip of an applicator containing silver nitrate/potassium (25%/75%, Grafco, Atlanta, GA, USA) to the center of the cornea steadily for eight seconds. Excess nitrate was washed with PBS after cauterization. Each mouse was treated for only one eye. Eye drops containing gp91 or GNP-gp91 were diluted in PBS to a final gp91 peptide concentration of 100 μg/mL. Five microliters of eye drops were applied to the mouse ocular surface once every two days for 7 days. The burn stimulus response and severity of corneal neovascularization were observed using a handheld portable slit lamp (SL-17, Kowa Company Ltd., Torrance, CA, USA) and photographed. The corneal neovascularization area was quantified using ImageJ software and presented as the percentage of the vessel area to the non-vessel area.

### Histological Examination

After 1 week of treatment, the mouse eyes were harvested and fixed in 10% formalin. The fixed eyes were individually embedded in paraffin and cut into 5 μm-thick sections. The sections were stained with hematoxylin and eosin and observed by a slide-based tissue cytometry (Axio Observer Z1, Tissue Gnostics, Vienna, Austria).

### Angiogenic Factors Examination from Cornea Lysate

The mouse corneas were isolated and weighed. Corneal tissues (four corneas/group from two batches) were harvested and homogenized with protein extraction buffer (Thermo Fisher Scientific). The mixture from each sample was centrifuged at 10,000 *g* for 3 minutes at 4 °C and the supernatant was collected. Total protein was quantified using Bradford assay (p010, GeneCopoeia, Rockville, MD, USA). Mouse nicotinamide adenine dinucleotide phosphate oxidase 2 (Nox2) ELISA Kit (My BioSource, cat no. MBS269961) was used to quantify Nox2 content in cornea. The angiogenic cytokines (MMP2, MMP9, and VEGF) content in each group was measured using the Quantikine® ELISA kit and Mouse VEGF/total MMP9/MMP2 Immunoassay (R&D Systems, Minneapolis, MN, USA) in triplicate. The experiments were conducted according to the manufacturer's protocol.

## Statistical Analysis

All data are presented as the mean ± standard deviation (SD). Experiments were additionally repeated to confirm reproducibility. Statistical differences between groups were analyzed using one-way ANOVA, followed by Tukey's post-hoc test using SPSS 17.0 (SPSS, Inc., Chicago, IL, USA). Statistical significance was set at $p < 0.05$.

# Results

## Characterization of GNP and GNP-gp91

Table 1 and Figure 2 are the results of the characterization of GNP and GNP-gp91. As shown in Table 1, when using gelatin solutions with pH 8, the average size of GNP and GNP-gp91 were 349.6 ± 25.8 and 550.6 ± 61.2 nm and the average zeta (ζ) potential of GNP and GNP-gp91 were −18.9 ± 1.0 mV and 21.7 ± 1.8 mV. When using gelatin solutions with pH 9, the average size of GNP and GNP-gp91 were 393.0 ± 44.2 nm and 483.2 ± 41.9 nm and the average zeta potential of GNP and GNP-gp91 were −20.2 ± 0.8 mV and 21.7 ± 0.9 mV. The encapsulation efficiency (EE) of gp91 in the GNP-gp91 was higher at pH 8 (79.4% ± 8.0%) than at pH 9 (44.8% ± 39.5%). Therefore, gelatin solutions with pH 8 was chosen to prepare GNP-gp91 for the subsequent experiments. Both GNP and GNP-gp91 with low PDI values (0.08~0.15) had a narrow size distribution (Table 1). The Size and Zeta potential patterns of GNP and GNP-gp91 are

**Table 1** Characterization of GNP and GNP-gp91 Prepared in Variant pH

| $pH_{gelatin}$ | Sample | Size (nm) | Zeta Potential (mV) | PDI | EE (%) |
|---|---|---|---|---|---|
| 8 | GNP | 349.6 ± 25.8 | −18.9 ± 1.0 | 0.08 ± 0.02 | / |
| | GNP-gp91 | 550.6 ± 61.2 | 21.7 ± 1.8 | 0.11 ± 0.03 | 79.4 ± 8.0 |
| 9 | GNP | 393.3 ± 44.2 | −20.2 ± 0.8 | 0.10 ± 0.03 | / |
| | GNP-gp91 | 483.2 ± 41.9 | 21.7 ± 0.9 | 0.15 ± 0.03 | 44.8 ± 39.5 |

**Note**: Data presented as mean ± standard deviation (n = 3).
**Abbreviations**: $pH_{gelatin}$, pH of gelatin solution during synthesis; Size, average hydrodynamic diameter; PDI, polydispersity index; EE, encapsulation efficiency of gp91.

shown in Figure 2A revealing single and narrow peak pattern in each group. The monodispersed colloidal solution of GNP and GNp-gp91 is shown in Figure 2B. From the TEM image, the synthesized GNP-gp91 showed no aggregation with spherical and smooth morphology, which also exhibited good dispersion (Figure 2C). In Figure 2D, the in vitro release profiles of gp91 and GNP-gp91 in PBS at pH 7 is revealed. The releases of gp91 and GNP-gp91 were 95.70% and 21.58% after 240 hours, respectively. This result demonstrated that gp91 was release faster than GNP-gp91. The gp91 loaded in GNP exhibited a slower peptide release behavior.

## GNP-gp91 Improves Uptake into Cells, Impairs Cell Viability, and Reduces ROS Production in the Cultured Endothelial Cells

To investigate the effect of gp91 in different formulations in vitro, the uptake rate of gp91 and GNP-gp91 was evaluated. FITC-labeled peptide ($gp91^{FITC}$) and GNP-$gp91^{FITC}$ were tested in HUVECs and compared against the uptake of the peptide using flow cytometry (Figure 3A). In 0.5 and 2 hours, the fluorescence peak of GNP-$gp91^{FITC}$ was shifted to the right showing high fluorescent intensity (Figure 3A). The quantification result is revealed in Figure 3B. The mean fluorescence intensities (MFI) of HUVECs treated with GNP-gp91 for 0.5 and 2 hours were 76,945 and 138,545 MFI (Figure 3B), respectively. This is much higher in the GNP-gp91 treated cells compared in the $gp91^{FITC}$- group (*$p < 0.05$).

The angiogenic assays including cell viability, migration, and tube formation were performed using HUVECs. For cell viability test, the gp91 content was adjusted to the same concentration as in the gp91 and GNP-gp91 groups. The same gelatin concentration of GNP was used to elucidate the effects of the nanoparticles. At gp91 concentrations ranging from 50~150 μg/mL, cell viability of all groups was greater than 85% and no significant difference compared with the control group (100%) (Figure 3C, Day 1). According to the cytocompatibility standards of ISO 10993–5, it indicated that all formulations have good cytocompatibility (>70%) at gp91 peptide concentration of 100 μg/mL. Along with increased peptide concentration and extended culture period, the cell viability of GNP-gp91 treated group started to decrease significantly. After 3 days of treatment, the GNP-gp91 group at a peptide concentration of 150 μg/mL showed the highest reduction in cell viability at 56.6% ± 11.6%, which was significantly lower than the same particle concentration of GNP (79.6% ± 9.8%) and peptide concentration of gp91 (89.49 ± 4.56%) groups (Figure 3C, Day 3). At lower gp91 concentration (100 μg/mL), cell viability value (70.82 ± 12.49%) revealed that acceptable cyto-compatibility was observed in the GNP-gp91 group (Figure 3C, Day 3); therefore, this peptide concentration was selected for further experiments. Images of HUVECs labeled with the live/dead stain are shown in Figure 3D. Live cells exhibited green color and dead cells revealed in red fluorescence, respectively. A large number of live cells showed green fluorescence in all the tested groups at a peptide concentration of 100 μg/mL on day 3 including GNP-gp91. However, more red fluorescent spots were also observed in the GNP-gp91 treated one. These results indicated that GNP-gp91 (100 μg/mL) was a little bit toxic to influence HUVECs. This result is in line with the Cell viability result.

The ROS content in LPS-induced inflamed cells treated with the variant formula is shown in Figure 3E. The ROS level in the control cells (basal medium) was used as the standard (100%). After LPS stimulation, ROS levels increased (1.5 folds). The ROS content in the GNP-, gp91- and GNP-gp91-treated cells was reduced, and the ROS value of GNP-gp91 was the lowest one (1.2 folds). The GNP-gp91 possessed capacity to reduce ROS content in inflamed cells, although there is no obviously differences here.

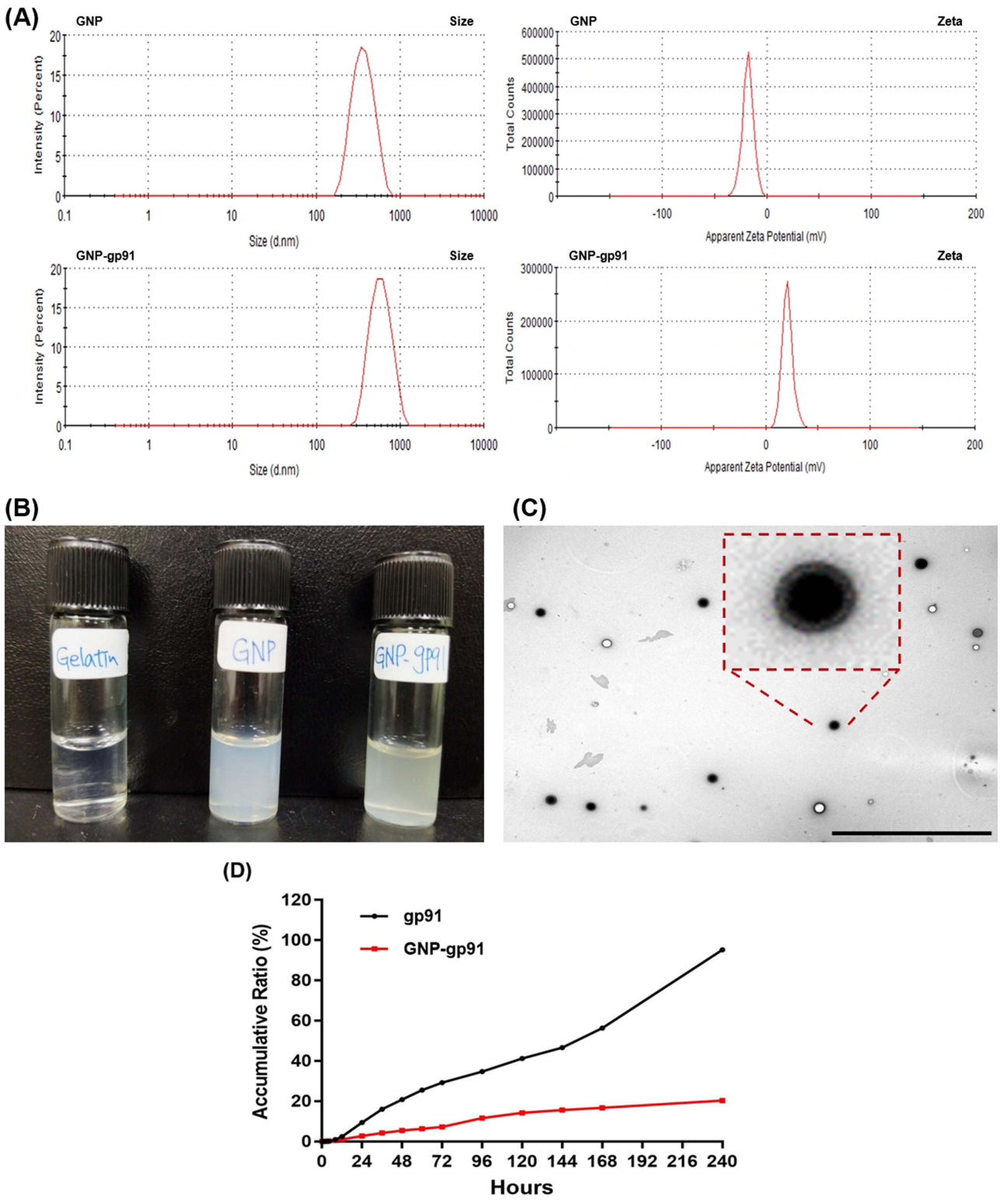


**Figure 2** Characterization of GNPs and GNP-gp91. (**A**) DLS results of size and zeta potential of GNP and GNP-gp91 at pH8. (**B**) Photograph of gelatin solution and GNP/GNP-gp91 colloidal solutions. (**C**) TEM image of GNP-gp91, scale bar: 10 μm. (**D**) The cumulative drug release profile of gp91 and GNP-gp91 in PBS at pH 7. Data are expressed as mean ± SD, n = 3.

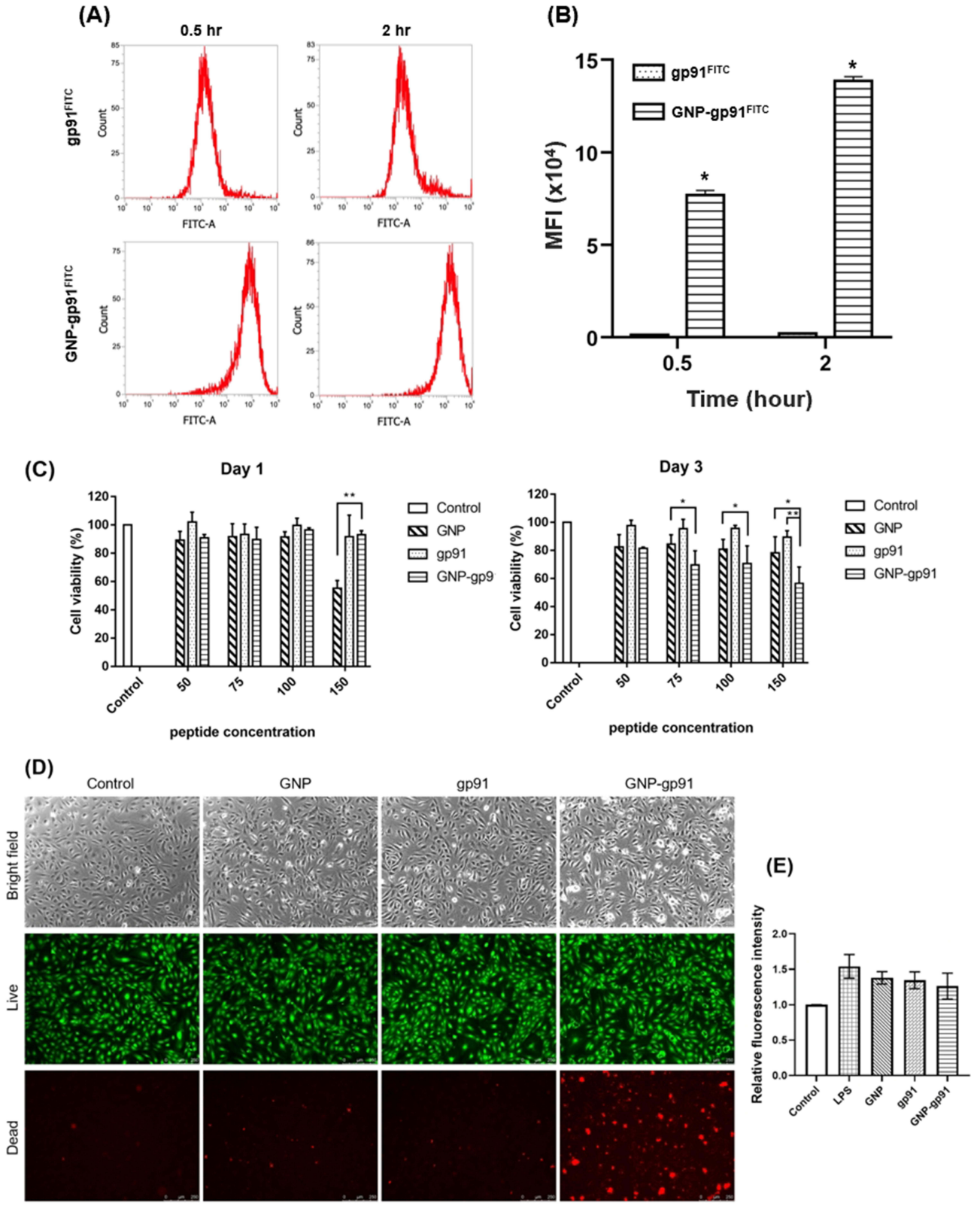


**Figure 3** Cell interaction with GNP-gp91. (**A**) Flow cytometric histograms of gp91$^{FITC}$- and GNP-gp91$^{FITC}$-treated cells, and (**B**) its quantification data of intracellular MFI (n = 3, *$p < 0.05$, compared with gp91$^{FITC}$). (**C**) Cell viability of HUVECs incubated with variant formulation at gp91 concentration from 50 to 150 μg/mL on day 1 and day 3 (n = 5, *$p < 0.05$, **$p < 0.01$). (**D**) Representative images of Live/Dead staining of HUVECs cultured with variant peptide formula (100 μg/mL) acquired on day 3, scale bar: 250 μm. (**E**) ROS changes in LPS-induced inflamed cells. (n = 3).

## GNP-gp91 Attenuates the Angiogenic Capacity in the Cultured Endothelial Cells

The scratch wound healing assay and Matrigel$^{TM}$-based tube formation assay were used to evaluate the anti-angiogenic effects of the various formulations. As shown in Figure 4A, HUVECs migrated into the gap after 6–8 hours in the control group. The wound closure rate after 8 hours in the control, GNP, gp91, and GNP-gp91 groups were 43.9% ± 0.3%, 45.1% ± 0.8%, 45.5% ± 2.7%, and 34.4% ± 2.6%, respectively (Figure 4B). This result implied that GNP-gp91 significantly inhibited the migratory capability of HUVECs (*$p < 0.001$). When HUVECs were cultured on Matrigel$^{TM}$ for 8 hours, capillary-like tubular structures were observed in the control group and the GNP-treated group (Figure 4C). However, fewer capillary structures were observed in the gp91 treated cells. Almost no mesh-like structure was found in the GNP-gp91-treated cells (Figure 4C). Overall, these results demonstrate that GNP-gp91 can effectively inhibit angiogenic activity in vitro.

## The Retention and Location of GNP-gp91 on Mice Ocular Surface

To confirm whether nanoparticle-containing eye drops can prolong the drug retention on the ocular surface, TAMRA-SE, a red fluorescent dye, was conjugated with GNPs to explore the accumulation and distribution of nanoparticles on the ocular surface by tracking fluorescent signals. Representative photographs of eyes from mice treated with various eye drops with dye (TAMRA) examined by the IVIS imaging system are shown in Figure 5A and Figure 5C. In normal mice, the eye treated with GNP-gp91 contained eyedrops exhibited higher fluorescence intensity (55.2%) than those treated with GNP (30.8%) and free dye solution (22.5%) for 10 min (Figure 5B). Subsequently, the highest fluorescence intensity was still recorded in the GNP-gp91 group; even after 80 min of exposure, there is 36.4% retention on ocular surface (Figure 5B). However, the free dye (TAMRA) group was <10%. We performed the same test on the eyes of corneal NV mice on day 7 (Figure 5C). The relative fluorescent percentage examined from the corneal NV mice (Figure 5D) is much higher than normal eyes. For example, the relative fluorescent intensity of GNP-gp91 is around 180% at 10 min, but the tendency of fluorescence intensity changes in these tested groups was similar to that in the normal and neovascularized cornea. The GNP-gp91 group showed the highest fluorescence intensity in the neovascularized cornea, whereas TAMRA (free dye) group was the lowest (Figure 5D). These data suggest that GNP-gp91 eyedrops can prolong the retention on the ocular surface.

To confirm the location of NPs, corneal cryosections were examined using a fluorescence microscope. Strong blue belt staining shows the cell nuclei of the corneal epithelial layers (Figure 5E, DAPI). Intensive red fluorescence was observed in the corneal epithelium (Ep) of the GNP-gp91 group (Figure 5E, TAMRA), weak signals were observed in the GNP group, and no red fluorescence signal was observed in the free dye (TAMRA) group (Figure 5E). The results provided direct evidence of high accumulation and longer retention of GNP-gp91 on the ocular surface and proofed its localization in the corneal epithelium.

## Therapeutic Efficacy of GNP-gp91 for Treating Corneal Neovascularization

Chemically burned corneal neovascularization models of mice were performed to evaluate the therapeutic effect of GNP-gp91 eye drops. Various eye drops were administered once every two days for seven days. The photographs captured under the slip lamp showed a smooth and transparent cornea in the normal eye (Figure 6A, control). Radial growth of blood vessels arising from the limbus towards the central burn area was observed in the PBS group. In contrast, fewer and thinner vessels were observed in both the gp91 and GNP-gp91 groups (Figure 6A), and the corneal area in the GNP-gp91 treated eye showed better transparency with almost no vessel formation (Figure 6A). The area of newly grown vessels was quantified and represented as the neovessel's ratio compared to the entire eyeball area (Figure 6B). Treatment group treated by GNP-gp91 showed a significantly lower neovessel percentage (7.89 ± 0.76%) than PBS (33.99 ± 2.94%) and gp91 (19.67 ± 1.04%) groups (**p < 0.001). The GNP-gp91 can significantly inhibit vessel formation in chemical-burned cornea even in the dosing frequency of every two-day interval.

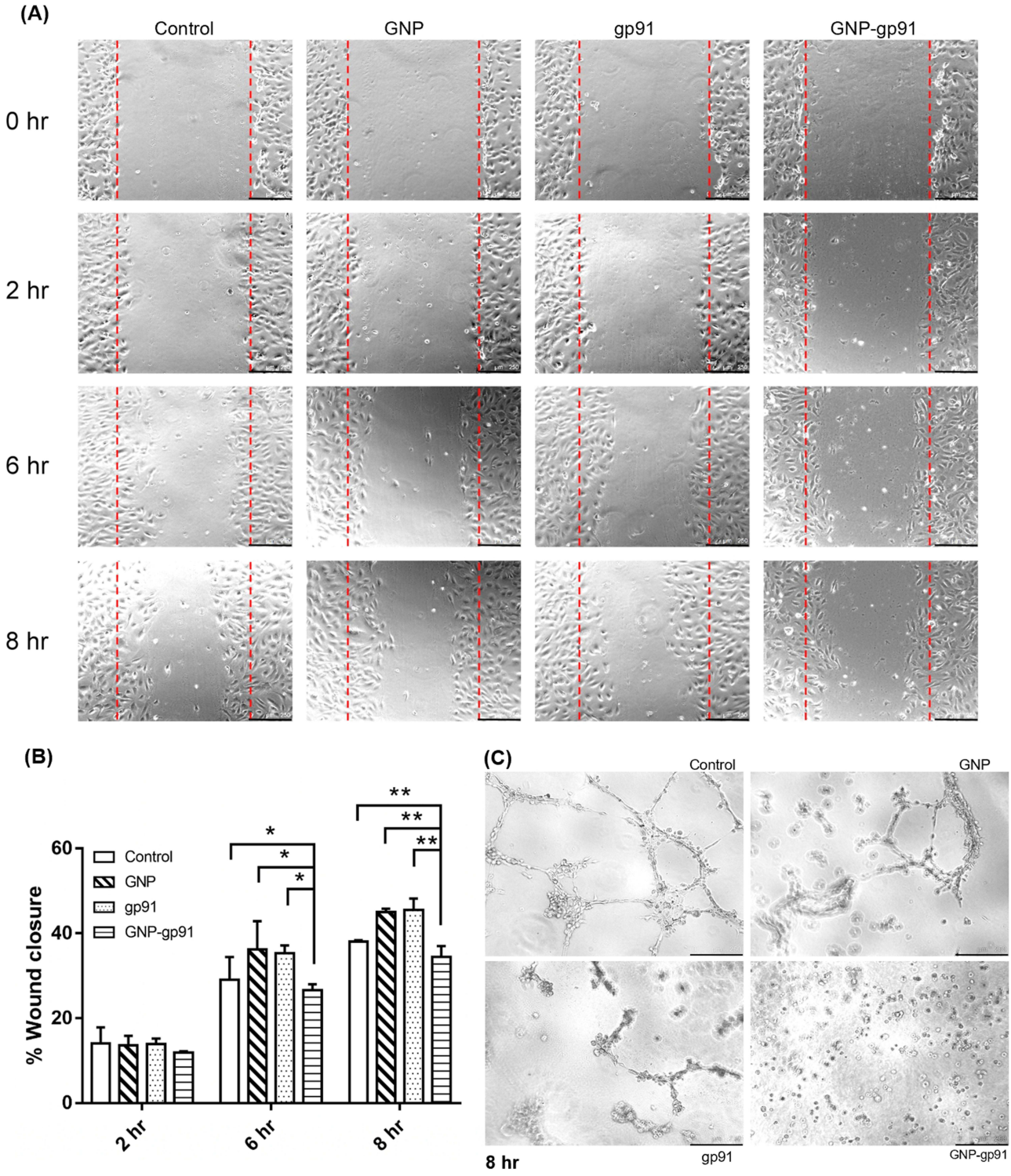


**Figure 4** Effects of GNP-gp91 on cell migration and tube formation. (**A**) Representative photos from wound healing assay of HUVECs treated with GNP, gp91, and GNP-gp91. Scale bar: 250 μm. (**B**) Quantification of wound closure rate at the indicated times (n = 3), *$p < 0.05$, **$p < 0.001$ compared with GNP-gp91 group. (**C**) Representative images of tube formation after culturing for 8 h, scale bar: 250 μm.

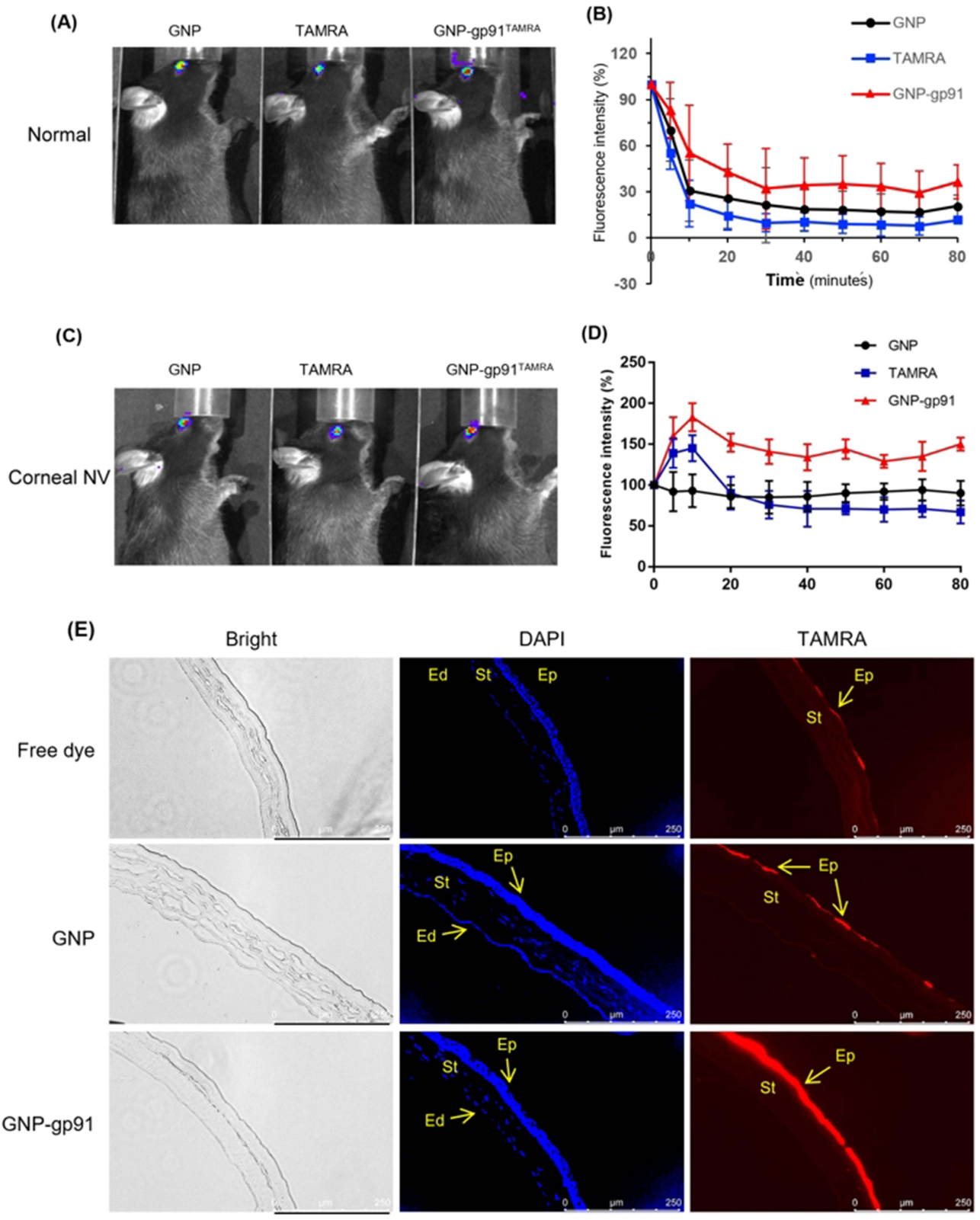


**Figure 5** Ocular retention and distribution of GNP-gp91. (**A**) Photo to show fluorescence accumulated on normal mice eye treated by $GNP^{TAMRA}$, free dye (TAMRA), and GNP-$gp91^{TAMRA}$ after 10 minutes dosing, and (**B**) its intensity variation curve changed with time. (**C**) Photo of neovascularized mice eye treated by variant fluorescent formulation after 10 minutes dosing, and (**D**) its intensity variation curve changed with time. Data are presented as mean ± SD (n = 3). (**E**) Corneal cryosections revealing the distribution of free dye, $GNP^{TAMRA}$, and GNP-$gp91^{TAMRA}$ in cornea (yellow arrow in TAMRA images indicated dye or NPs location). Scale bar: 250 μm. Corneal epithelium: Ep, Stroma: St, endothelium: Ed.

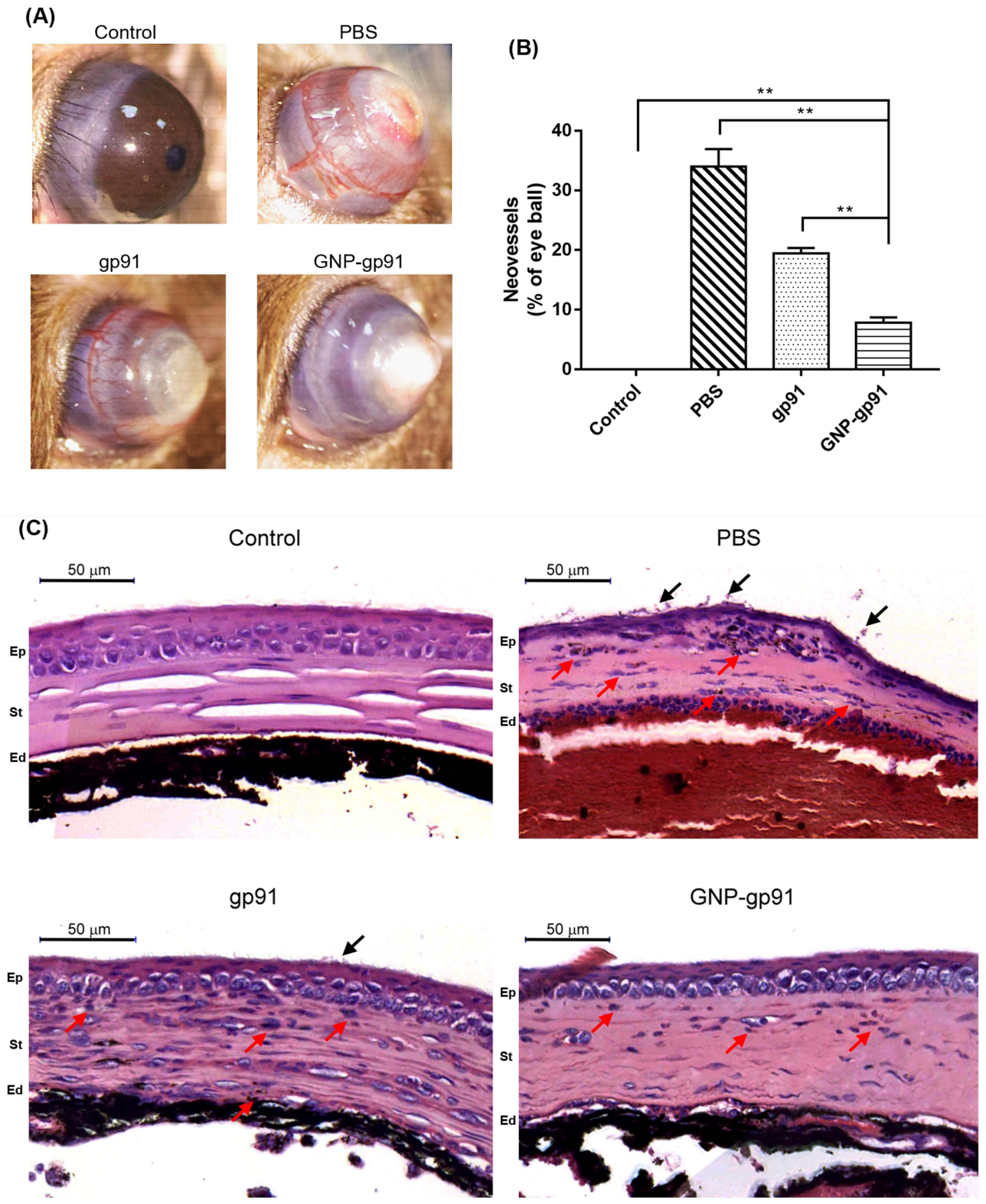


**Figure 6** Eyedrops containing GNP-gp91 can inhibit vessel formation in chemical cauterization-induced corneal neovascularization. (**A**) Representative images of cornea from normal eye, and PBS, gp91, and GNP-gp91NP-treated corneal NV. (**B**) The area of blood vessels in the cornea was quantified using Image J software. Data are presented as mean ± SD (Normal: n = 3. PBS, gp91, and GNP-gp91: n = 6). $^{**}p < 0.001$ compared with GNP-gp91 group. (**C**) Histological assessment of central corneal sections after 7 days treatment. Inflammatory cell infiltrating into the stroma (red arrows) and exhibiting defective corneal epithelium (black arrows) was observed in the PBS group compared with the control group. Epithelium: Ep, stroma: St, endothelium: Ed.


https://doi.org/10.2147/IJN.S398769 DovePress

Histopathology of the corneal tissues was examined under a microscope by H&E staining. Representative images of the central cornea are shown in Figure 6C. The corneal surface of normal mice was smooth, and the epithelium (Ep) was integral. In the damaged cornea, the epithelial layer became thinner, the epithelium was exfoliated, and many inflammatory cells were found in the stroma (St) in the PBS- and gp91-treated groups after seven days. In the GNP-gp91-treated eye, cauterized corneas with relatively intact epithelium and fewer inflammatory cells in the stroma were observed (Figure 6C), which is similar to the normal cornea, were observed.

## Reduction of Angiogenic Factors in Cornea

The gp91 peptide can mediate Nox2 and ROS, then influencing angiogenesis; therefore, the Nox2 content in cornea was examined. Corneal neovascularization is associated with several angiogenic factors such as VEGF and MMPs, and these factors were also quantified. The protein level of VEGF, MMP2, and MMP9 in control cornea were 9.20 ± 3.81 pg/mL, 38.99 ± 4.93 ng/mL, and 15.57 ± 0.27 ng/mL (Figure 7A–D), respectively. The PBS-treated cornea showed higher concentration of Nox2 (1.01 ± 0.01 ng/mL), VEGF (183.21 ± 3.47 pg/mL), MMP2 (65.21 ± 0.02 ng/mL), and MMP9 (207.23 ± 9.74 ng/mL), which were higher than the control group (normal cornea). The gp91 group showed similar results to those of the PBS group, and it had no effect on the reduction in MMP9 and MMP2 levels (Figure 7C and Figure 7D). In the GNP-gp91-treated group, the Nox2 level (0.53 ± 0.03 ng/mL) and VEGF level (72.22 ± 0.04 pg/mL) were the lowest in all tested groups (Figure 7A and Figure 7B), and these''re statistical difference with PBS- or gp91-treated groups (**$p < 0.05$). The MMP2 concentration in the GNP-gp91-treated one is the lowest (53.81 ± 10.86 ng/mL) in all tested groups (Figure 7D).

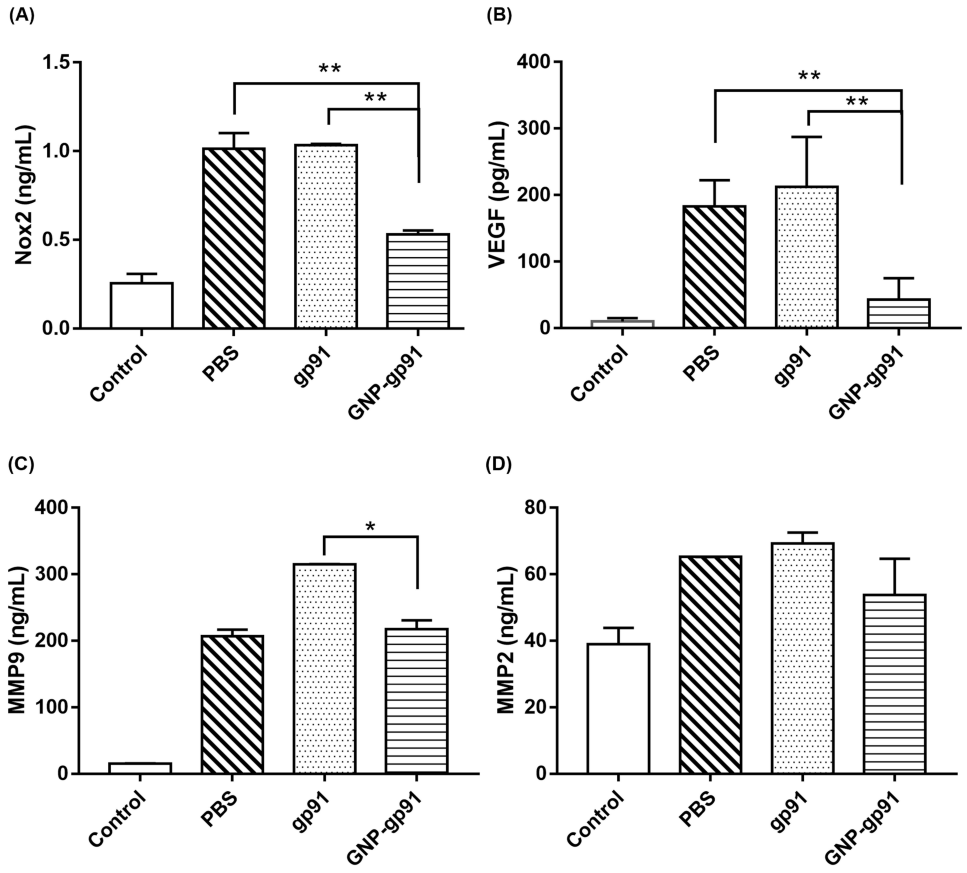


**Figure 7** Quantification of angiogenic cytokines from cornea protein lysate. Mice received chemical cauterization and were treated with PBS, gp91, and GNP-gp91 eye drops. Quantification of (**A**) Nox2, (**B**) VEGF, (**C**) MMP9, and (**D**) MMP2 levels from the cornea lysates. Data are presented as mean ± SD (n = 3), *$p < 0.05$, **$p < 0.001$ compared with GNP-gp91 group.

## Discussion

Corneal neovascularization is also a common cause of blindness worldwide.[3,4,35] The majority of corneal neovascularization cases involve inflammatory conditions at an early stage, and VEGF is the major factor involved in the development of neovascularization. Although steroids and anti-VEGF agents have been used to suppress corneal neovascularization in clinics, serious side effects such as hypertension, cataracts, or delayed wound healing have revealed that alternative therapeutic agents are needed. In this study, we demonstrated that the nanomedicine, gp91 tat peptide loaded in gelatin nanoparticles (GNP-gp91), can effectively inhibit the migration and tube formation capacity of HUVECs and can also be used as eye drops to reduce vessel formation in mice with corneal neovascularization induced by chemical injury.

Gelatin can be extracted using acidic/alkaline processes to prepare type A and type B gelatin from collagen. At pH 6~7, type A gelatin has a positive net charge, while type B gelatin is negatively charged.[36] The gp91 tat peptide with high amount of arginine and lysine residues possesses positively charged;[37] therefore, using type B gelatin can have charge interaction to form strong attraction between gelatin and gp 91 peptides. For gelatin nanoparticle (GNP) preparation, pH value of the prepared gelatin solution is considered as one of the critical factors that affects the structure, conformation, and charge properties of gelatin,[38–40] further influencing the formation and stability of GNP.[39,40] In addition, glutaraldehyde was used as a crosslinker in the study, and it is reported that a better cross-linking degree will be obtained under higher pH conditions (alkaline conditions: pH 8–10).[41,42] Owing to the isoelectric point (PI) of gp91 is around 12.5–13.0 (calculated by the website of Expasy and Prot pi-Peptide Tool); therefore, to maintain the amino group on gp91 protonated lead to non-participating in the crosslinking reaction, we just investigated the synthesis under pH 8 and pH 9. As shown in Table 1, the GNP fabricated using gelatin solution at pH 8 had a smaller particle size than at pH 9 and a negative zeta potential at −18.9 mV. However, after loading the gp91 peptide into GNP, a substantial change in size was observed, accompanied by a positive zeta potential at 21.7 mV at pH 8. Of these 18 amino acids of the gp91ds-tat peptide, 11 were positively charged arginine and lysine residues,[37] resulting in this peptide becoming a positively charged peptide. Therefore, the zeta potential of GNP changed from negative (−19 mV) to positive after gp91 loading (GNP-gp91, approximately 22 mV). As shown in Table 1, the encapsulation efficiency (EE) under pH 8 and pH 9 is 79.4% and 44.8%, respectively. Owing to non-participating in the crosslinking reaction, the encapsulation efficiency of gp91 will depend on the compactness of GNP and ionic interaction. In theory, a better crosslinking efficiency will be obtained under pH 9. Therefore, the result here indicated that a higher encapsulation efficiency under pH 8 is because the charge of gp91 will be more positive resulting in the ionic interaction between gp91 and crosslinker gelatin being stronger. The release of peptide in solution (gp91) was faster, and slow release of peptide from GNP-gp91 was observed (Figure 2D). The drug release mechanism from GNP is reported including 3 steps: (1) simple diffusion of drug particles, (2) degradation release, and (3) cleavage of the gelatin matrix by proteolytic enzymes.[28] In this study, gp91 peptide was mixed with a gelatin solution before GNP preparation. Therefore, the gp91 peptide was homogeneously distributed in the nanoparticle matrix (Figure 2C and Table 1, low PDI) and was not easily released by simple diffusion with no burst release (Figure 2D) compared to the release profile of human serum albumin-loaded GNP.[43] When the diffusion of the drug is lower than matrix degradation, the mechanism of drug release mainly depends upon degradation.[28] Gelatin is enzymatically degraded into amino acids as a function of parameters such as pH, temperature, or concentration.[27] A controllable system with constant release of GNP-gp91via gelatin degradation in buffer for a longer time, as well as cleavage by lysozyme in cells can be predicted.

For cellular uptake, generally, gp91, a cell-penetrating peptide, could also exhibit a favorable cellular uptake efficiency. However, in Figure 3A and Figure 3, a higher cellular uptake efficiency of GNP-gp91 was founded, and this is facilitated by gelatin which could further specifically bind to collagen receptors and enter into cells through clathrin-dependent endocytosis.[44] The gp91ds-tat has shown to suppress both oxidative stress and cytokine production, which may have significant neuroprotective effects.[12,45] It also effectively attenuated ischemia/reperfusion-induced myocardial injury by inhibiting ROS release.[45,46] Hachisuka et al reported that gp91ds-tat treatment reduced new blood vessel formation in a tissue-engineering chamber.[47] However, whether gp91ds-tat plays an important role in the treatment of corneal NV is unknown. We found that gp91ds-tat nanoparticles (GNP-gp91) at a peptide concentration

<100 μg/mL had no toxic effects on HUVECs via cell viability assay on day 1 and day 3 (Figure 3C). But when gp91 peptide concentration reaching 150 μg/mL, the cell viability of GNP-gp91 on day 3 was down to around 50%. This may result from the endocytosis of GNP-gp91 getting high amount of drug intracellular (Figure 3A and Figure 3) and slow-release of gp91 to cause long-term effect (Figures 2D and 3C-day 3). The Live/Dead staining results showed that after 3 days of treatment with GNP-gp91 (100μμg/mL), some dead cells were observed (Figure 3D) due to the effect of gp91. Nox is an effector involved in VEGF signaling in pathological angiogenesis.[48,49] Nox2 is known to be abundantly expressed in vascular and inflammatory cells and is important for angiogenesis through the production of ROS.[50,51] Despite there is no significant difference between these formulations, the average ROS amount for the GNP-gp91 was the lowest (Figure 3E) showing this gp91-nanoformulation has potential to reduce ROS content in cells.

To further confirm its ability to inhibit angiogenesis, GNP-gp91 was evaluated in in vitro via wound healing and tube formation assays. GNP-gp91 group remarkably suppressed cell recovering to the gap area (Figure 4A and Figure 4) and tube formation (Figure 4C) of HUVECs compared to GNP group and gp91 group. These results indicated that gp91 carried by GNP-gp91 remained higher peptide concentration and certain peptide activity for working on HUVEC cells and influencing its function.

Positively charged NPs can interact with the negatively charged mucin layer of the tear film, which extends the retention time and absorption on the ocular surface.[29,36,52–54] The IVIS results showed that the GNP-gp91 group had higher retention properties than the free dye (TAMRA) and GNP group in normal and corneal NV mice (Figure 5A–D). We also observed the distribution via fluorescence microscopy, and the GNP-gp91 group demonstrated obvious fluorescence in the corneal epithelium compared with the GNP group and free dye group (Figure 5E), which is in line with expectations.

Recent studies demonstrate that Nox1, Nox2, and Nox4 modulate retinal and choroidal neovascularization via VEGF signaling.[49,55–57] Alkali-burned corneas were found to markedly upregulate the transcription and expression of *NOX2* and *NOX4* in human and mouse corneas.[58,59] Chan et al found that cauterizing a mouse cornea with a nitrate stick to cause vascularization led to an increase in the mRNA expression of *NOX2*, which also causes an increase in *VEGFA, VEFGR1*, and *VEGFR2*.[59] A similar result was observed in the present study. Interestingly, we have observed a high level of Nox2 and VEGF protein (Figure 7A and 7B) in the alkali-burned mice cornea treated with gp91. This may result from the lower amount of peptide accumulating on the ocular surface (Figure 5) and not easily get intracellular to effect cells (Figures 3A and 5E), then no effective function for inhibiting tube formation (Figure 4C) and vessel formation in cornea (Figure 6, gp91 group). Similarly, topically administered bevacizumab shows poor penetration through the corneal epithelium owing to tight intracellular junctions.[60] Therefore, the topical administration of gp91ds-tat requires a more efficient drug delivery system such as GNP to improve therapeutic efficacy. For the ocular retention test, relative higher fluorescence intensity (especially GNP-gp91) accumulated on the damaged ocular surface (Corneal NV, Figure 5C and Figure 5) than normal cornea (Figure 5A and Figure 5). This tendency is in accordance with the study of L.D, Huang et al revealed in 2021, that large amount of bromo-heptadecafluorooctane and tetrandrine which loaded in liposome can be remained on ocular surface and accumulated in the corneal epithelium of dry eye rabbit ; this apperance was caused by inflamed corneal cells uptaken more liposome nanoparticles into damage cornea.[61]

In the present study, we further showed that block NOX2 signaling by GNP-gp91 substantially reduced the protein expression of Nox2, VEGF, MMP2, and MMP9 (Figure 7). Activation of Nox2 requires a combination of p47phox, p67phox, p40phox, and Ras-related C3 botulinum toxin substrate 1 (Rac1).[62] gp91ds-tat prevents the interaction of p47phox with Nox2 and membrane subunits (gp91phox and p22phox) and inhibits $O_2^-$ formation.[37,62] High oxidative stress can impair endothelial cell function and angiogenesis as well as Nox2 and ROS production.[63] ROS production by Nox2 activation contributes to various pathologies, such as diabetes and hypertension.[64] gp91ds-tat has been reported to reverse insulin resistance-induced impairment of endothelial cells.[64] Zuo et al reported that targeting VEGF therapy in alkali burn-induced mouse corneal NV was beneficial in reducing the expression of vascular areas and the number of new vessels.[65] Kvanta et al revealed high expression of MMP2, MMP9, and VEGF in a rat model of inflammation-associated corneal neovascularization.[66] The effective inhibition of NV in the cornea of GNP-gp91 eye drops is attributed to 1) high retention and accumulation of cationic NPs in the cornea and uptake by cells (Figures 2A, 2B and 5) and 2) slow release to lasting peptide bioavailability in the cornea even at low dosing frequency (every two days) (Figures 2D and 3C). The

last, released gp91 peptide affected Nox2 and ROS activity, thereby inducing a cascade inhibition of angiogenesis (Figures 3E, 4, 6 and 7).

From the presented study's perspective, topical application of gp91 peptide in nanoparticle formulations could be a feasible way for the treatment of corneal neovascularization.

## Conclusions

In summary, gp91ds-tat peptide-loaded GNP (GNP-gp91) was successfully synthesized at a size of 550 nm and zeta potential of approximately 22 mV under colloidal conditions (PDI < 0.15) prepared from gelatin solution at pH 8. It showed a slow-release profile of GNP-gp91. High cell viability and non-toxicity of HUVECs when gp91 concentration <100 μg/mL in variant peptide formulation was proofed even GNP-gp91. This nanomedicine, GNP-gp91, substantially inhibited HUVEC wound healing and tube formation capacity at a peptide concentration of 100 μg/mL after 8 h treatment. GNP-gp91 can be easily captured on the ocular surface and possesses a longer retention time to reduce the dosing frequency when delivered topically (eye drops) every two days. Topical application of GNP-gp91 as eye drops can suppress the corneal neovascularization in a mouse model of chemically burned eye, and result with less vessel area formation in cornea (8%) was obtained when compared with PBS group (34%) and gp91 group (20%). Overall, our data indicate that GNP-gp91 nanomedicine contained eye drops has the potential to effectively treat corneal neovascularization in a low dosing frequency, which is effective and friendly to patients for clinical us.

## Funding

This work was supported by grants from the Ministry of Science and Technology, Taiwan (grant number: MOST 106-2628-E-038 -001 -MY3 and MOST 110-2314-B-038 -044 -MY2). This work was also partially supported by a grant from the Integrated Research Grant in Health and Medical Sciences from the National Health Research Institute, Taiwan (NHRI-EX111-10933SI).

## Disclosure

The authors declare no conflicts of interest.

## References

1. Zhang C, Yin Y, Zhao J, et al. An update on novel ocular nanosystems with possible benefits in the treatment of corneal neovascularization. *Int J Nanomedicine*. 2022;17:4911–4931. doi:10.2147/IJN.S375570
2. Britton Anna K, Crayford Basil B. Resolution of refractory corneal neovascularization with subconjunctival bevacizumab. *Case Rep Ophthalmol*. 2020;11:652–657. doi:10.1159/000510114
3. Sharif Z, Sharif W. Corneal neovascularization: updates on pathophysiology, investigations & management. *Romanian J Ophthalmol*. 2019;63:15–22. doi:10.22336/rjo.2019.4
4. Nicholas MP, Mysore N. Corneal neovascularization. *Exp Eye Res*. 2021;202:108363. doi:10.1016/j.exer.2020.108363
5. Brunner M, Romano V, Steger B, et al. Imaging of corneal neovascularization: optical coherence tomography angiography and fluorescence angiography. *Invest Ophthalmol Vis Sci*. 2018;59:1263–1269. doi:10.1167/iovs.17-22035
6. Hsu C-C, Chang H-M, Lin T-C, et al. Corneal neovascularization and contemporary antiangiogenic therapeutics. *J Chin Med Assoc*. 2015;78:323–330. doi:10.1016/j.jcma.2014.10.002
7. Roshandel D, Eslani M, Baradaran-Rafii A, et al. Current and emerging therapies for corneal neovascularization. *Ocul Surf*. 2018;16(4):398–414. doi:10.1016/j.jtos.2018.06.004
8. Al-Debasi T, Al-Bekairy A, Alkatheri A, Al Harbi S, Mansour M, Albekairy A. Topical versus subconjunctival anti-vascular endothelial growth factor therapy (Bevacizumab, Ranibizumab and Aflibercept) for treatment of corneal neovascularization. *Saudi J Ophthalmol*. 2017;31(2):99–105. doi:10.1016/j.sjopt.2017.02.008
9. Barry Z, Park B, Corson TW. Pharmacological potential of small molecules for treating corneal neovascularization. *Molecules*. 2020;25 (3468):1–40. doi:10.3390/molecules25153468
10. Feizi S, Azari A, Safapour S. Therapeutic approaches for corneal neovascularization. *Eye Vision*. 2017;4(28):1–10. doi:10.1186/s40662-017-0094-6
11. Rojas M, Lemtalsi T, Toque H, et al. NOX2-induced activation of arginase and diabetes-induced retinal endothelial cell senescence. *Antioxidants*. 2017;6(43):1–13. doi:10.3390/antiox6020043
12. Khayrullina G, Bermudez S, Byrnes K. Inhibition of NOX2 reduces locomotor impairment, inflammation, and oxidative stress after spinal cord injury. *J Neuroinflammation*. 2015;12:172. doi:10.1186/s12974-015-0391-8
13. Singh PK, Saadi A, Sheeni Y, Shekh-Ahmad T. Specific inhibition of NADPH oxidase 2 modifies chronic epilepsy. *Redox Biol*. 2022;58:102549. doi:10.1016/j.redox.2022.102549
14. Hu CG, Wu ZF, Huang ZH, et al. Nox2 impairs VEGF-A-induced angiogenesis in placenta via mitochondrial ROS-STAT3 pathway. *Redox Biol*. 2021;45:102051. doi:10.1016/j.redox.2021.102051

15. Ucgul RK, Celebi S, Yilmaz NS, Bukan N, Ucgul AY. Intrastromal versus subconjunctival anti-VEGF agents for treatment of corneal neovascularization: a rabbit study. *Eye*. 2021;35(11):3123–3130. doi:10.1038/s41433-020-01347-3
16. Fraunfelder FT. Chapter 2 - Ocular drug delivery and toxicology. In: Fraunfelder FFT, Fraunfelder FRW, editors. *Drug-Induced Ocular Side Effects*. 8th ed. London: Elsevier; 2021:3–11.
17. Loftsson T. Topical drug delivery to the retina: obstacles and routes to success. *Expert Opin Drug Deliv*. 2022;19(1):9–21. doi:10.1080/17425247.2022.2017878
18. Tian B, Bilsbury E, Doherty S, et al. Ocular drug delivery: advancements and Innovations. *Pharmaceutics*. 2022;14(9):1931. doi:10.3390/pharmaceutics14091931
19. Srividya G, Rapalli VK, Waghule T, et al. Nanocarriers for ocular drug delivery: current status and translational opportunity. *RSC Adv*. 2020;10:27835–27855. doi:10.1039/D0RA04971A
20. Joseph R, Venkatraman S. Drug delivery to the eye: what benefits do nanocarriers offer? *Nanomedicine*. 2017;12:683–702. doi:10.2217/nnm-2016-0379
21. Mun E, Morrison P, Williams A, Khutoryanskiy V. On the barrier properties of the cornea: a microscopy study of the penetration of fluorescently labeled nanoparticles, polymers, and sodium fluorescein. *Mol Pharm*. 2014;11:3556–3564. doi:10.1021/mp500332m
22. Zimmer A, Kreuter J. Microspheres and nanoparticles used in ocular delivery systems. *Adv Drug Deliv Rev*. 1995;16:61–73. doi:10.1016/0169-409X(95)00017-2
23. Yadav T, Jat RK. Microspheres as an ocular drug delivery system – a review. *J Drug Deliv Therap*. 2013;3:114–123. doi:10.22270/jddt.v3i1.343
24. Nagarwal R, Kant S, Singh P, Maiti P, Pandit J. Polymeric nanoparticulate system: a potential approach for ocular drug delivery. *J Control Release*. 2009;136:2–13. doi:10.1016/j.jconrel.2008.12.018
25. Zhu S, Gong L, Li Y, Xu H, Gu Z, Zhao Y. Safety assessment of nanomaterials to eyes: an important but neglected issue. *Adv Sci*. 2019;6(16):1802289. doi:10.1002/advs.201802289
26. Mobaraki M, Soltani M, Zare Harofte S, et al. Biodegradable nanoparticle for cornea drug delivery: focus review. *Pharmaceutics*. 2020;12(12):1–26. doi:10.3390/pharmaceutics12121232
27. Sahoo N, Sahoo R, Biswas N, Guha A, Kuotsu K. Recent advancement of gelatin nanoparticles in drug and vaccine delivery. *Int J Biol Macromol*. 2015;81:317–331. doi:10.1016/j.ijbiomac.2015.08.006
28. Yasmin R, Shah M, Khan S, Ali R. Gelatin nanoparticles: a potential candidate for medical applications. *Nanotechnol Rev*. 2017;6:191–207. doi:10.1515/ntrev-2016-0009
29. Huang H-Y, Wang M-C, Chen Z-Y, et al. Gelatin–epigallocatechin gallate nanoparticles with hyaluronic acid decoration as eye drops can treat rabbit dry-eye syndrome effectively via inflammatory relief. *Int J Nanomedicine*. 2018;13:7251–7273. doi:10.2147/IJN.S173198
30. Chuang YL, Fang HW, Ajitsaria A, et al. Development of Kaempferol-loaded gelatin nanoparticles for the treatment of corneal neovascularization in mice. *Pharmaceutics*. 2019;11(635):1–16. doi:10.3390/pharmaceutics11120635
31. Coester C, Langer K, Briesen H, Kreuter J. Gelatin nanoparticles by two step desolvation - A new preparation method, surface modifications and cell uptake. *J Microencapsul*. 1999;17:187–193.
32. Ofokansi K, Winter G, Fricker G, Coester C. Matrix-loaded biodegradable gelatin nanoparticles as new approach to improve drug loading and delivery. *Eur J Pharm Biopharm*. 2010;76(1):1–9. doi:10.1016/j.ejpb.2010.04.008
33. Kalyanaraman B, Darley-Usmar V, Davies K, et al. Measuring reactive oxygen and nitrogen species with fluorescent probes: challenges and limitations. *Free Radic Biol Med*. 2012;52:1–6. doi:10.1016/j.freeradbiomed.2011.09.030
34. Wang J-H, Tseng C-L, Lin F-L, et al. Topical application of TAK1 inhibitor encapsulated by gelatin particle alleviates corneal neovascularization. *Theranostics*. 2022;12:657–674. doi:10.7150/thno.65098
35. World Health Organization. Blindness and vision impairment; 2022. Available from: https://www.who.int/news-room/fact-sheets/detail/blindness-and-visual-impairment. Accessed March 10, 2023.
36. Tseng C-L, Chen K-H, Su W-Y, Lee Y-H, Wu -C-C, Lin F-H. Cationic gelatin nanoparticles for drug delivery to the ocular surface: in vitro and in vivo evaluation. *J Nanomater*. 2013;2013:1–11. doi:10.1155/2013/238351
37. Rey F, Cifuentes-Pagano E, Kiarash A, Quinn M, Pagano P. Novel competitive inhibitor of NAD(P)H oxidase assembly attenuates vascular $O^{2-}$ and systolic blood pressure in mice. *Circ Res*. 2001;89:408–414. doi:10.1161/hh1701.096037
38. Li Z, Gu L. Effects of mass ratio, pH, temperature, and reaction time on fabrication of partially purified pomegranate ellagitannin-gelatin nanoparticles. *J Agric Food Chem*. 2011;59:4225–4231. doi:10.1021/jf200024d
39. Ahsan S, Rao C. The role of surface charge in the desolvation process of gelatin: implications in nanoparticle synthesis and modulation of drug release. *Int J Nanomedicine*. 2017;12:795–808. doi:10.2147/IJN.S124938
40. Vinjamuri BP, Papachrisanthou K, Haware R, Chougule M. Gelatin solution pH and incubation time influences the size of the nanoparticles engineered by desolvation. *J Drug Deliv Sci Technol*. 2021;63:102423. doi:10.1016/j.jddst.2021.102423
41. Zhang T, Yu Z, Ma Y, Chiou B-S, Liu F, Zhong F. Modulating physicochemical properties of collagen films by cross-linking with glutaraldehyde at varied pH values. *Food Hydrocoll*. 2022;124:107270. doi:10.1016/j.foodhyd.2021.107270
42. Slusarewicz P, Zhu K, Hedman T. Kinetic characterization and comparison of various protein crosslinking reagents for matrix modification. *J Mater Sci Mater Med*. 2010;21(4):1175–1181. doi:10.1007/s10856-010-3986-8
43. Solanki P, Sajwan R. Gelatin nanoparticles as a delivery system for proteins. *J Nanomed Res*. 2015;2:18–20. doi:10.15406/jnmr.2015.02.00018
44. Potapovitch A, Suhan T, Shutava T, Kostyuk V. Receptor-mediated endocytosis is an important way for gelatin nano-particles penetration into cells. *J Belarusian State Univ Biol*. 2020;3–10. doi:10.33581/2521-1722-2020-1-3-10
45. Cifuentes-Pagano E, Meijles DN, Pagano PJ. The quest for selective nox inhibitors and therapeutics: challenges, triumphs and pitfalls. *Antioxid Redox Signal*. 2014;20(17):2741–2754. doi:10.1089/ars.2013.5620
46. DelBaugh R, Chen Q, Devine I, et al. Nox2ds-Tat, A Peptide Inhibitor of NADPH Oxidase, exerts cardioprotective effects by attenuating reactive oxygen species during ischemia/reperfusion injury. *Am J Biomed Sci*. 2016;8:208–227.
47. Hachisuka H, Dusting G, Abberton K, Morrison W, Jiang F. Role of NADPH oxidase in tissue growth in a tissue engineering chamber in rats. *J Tissue Eng Regen Med*. 2008;2:430–435. doi:10.1002/term.115
48. Xia C, Meng Q, Liu L-Z, Rojanasakul Y, Wang X-R, Jiang B-H. Reactive oxygen species regulate angiogenesis and tumor growth through vascular endothelial growth factor. *Cancer Res*. 2007;67:10823–10830. doi:10.1158/0008-5472.CAN-07-0783

49. Chan E, Wijngaarden P, Liu G-S, Jiang F, Peshavariya H, Dusting G. Involvement of Nox2 NADPH oxidase in retinal neovascularization. *Invest Ophthalmol Vis Sci*. 2013;54:7061–7067. doi:10.1167/iovs.13-12883
50. Fukai M. Redox signaling in angiogenesis: role of NADPH oxidase. *Cardiovasc Res*. 2006;71:226–235. doi:10.1016/j.cardiores.2006.04.015
51. Bedard K, Krause K-H. The NOX family of ROS-generating NADPH oxidases: physiology and pathophysiology. *Physiol Rev*. 2007;87:245–313. doi:10.1152/physrev.00044.2005
52. Tsai C-H, Wang P-Y, Lin IC, Huang H, Liu G-S, Tseng C-L. Ocular drug delivery: role of degradable polymeric nanocarriers for ophthalmic application. *Int J Mol Sci*. 2018;19(2830):1–20. doi:10.3390/ijms19092830
53. Castro B, Fulgêncio G, Domingos L, Cotta O, Silva-Cunha A, Fialho S. Positively charged polymeric nanoparticles improve ocular penetration of tacrolimus after topical administration. *J Drug Deliv Sci Technol*. 2020;60:101912. doi:10.1016/j.jddst.2020.101912
54. Des Rieux A, Fievez V, Garinot M, Schneider Y-J, Preat V. Nanoparticles as potential oral delivery systems of proteins and vaccines: a mechanistic approach. *J Control Release*. 2006;116:1–27. doi:10.1016/j.jconrel.2006.08.013
55. Li Q, Dinculescu A, Shan Z, et al. Downregulation of p22phox in retinal pigment epithelial cells inhibits choroidal neovascularization in mice. *Mol Ther*. 2008;16:1688–1694. doi:10.1038/mt.2008.164
56. Vogel J, Kruse C, Zhang M, Schröder K. Nox4 supports proper capillary growth in exercise and retina neo-vascularization: nox4 in exercise. *J Physiol*. 2015;593:2145–2154. doi:10.1113/jphysiol.2014.284901
57. Wilkinson-Berka J, Deliyanti D, Rana I, et al. NADPH oxidase, NOX1, mediates vascular injury in ischemic retinopathy. *Antioxid Redox Signal*. 2014;20:2726–2740. doi:10.1089/ars.2013.5357
58. Gu X-J, Liu X, Zhao Y, et al. Involvement of NADPH oxidases in alkali burn-induced corneal injury. *Int J Mol Med*. 2016;38:75–82. doi:10.3892/ijmm.2016.2594
59. Chan E, Wijngaarden P, Chan E, et al. NADPH oxidase 2 plays a role in experimental corneal neovascularisation. *Clin Sci*. 2016;130:683–696.
60. Dastjerdi M, Sadrai Z, Saban D, Zhang Q, Dana R. Corneal penetration of topical and subconjunctival Bevacizumab. *Invest Ophthalmol Vis Sci*. 2011;52:8718–8723. doi:10.1167/iovs.11-7871
61. Huang L, Gao H, Wang Z, Zhong Y, Hao L, Du Z. Combination nanotherapeutics for dry eye disease treatment in a rabbit model. *Int J Nanomedicine*. 2021;16:3613–3631. doi:10.2147/IJN.S301717
62. Brandes R. A radical adventure: the quest for specific functions and inhibitors of vascular NAPDH oxidases. *Circ Res*. 2003;92:583–585. doi:10.1161/01.RES.0000066880.62205.B0
63. Fukai M. VEGF signaling through NADPH oxidase-derived ROS. *Antioxid Redox Signal*. 2007;9:731–739. doi:10.1089/ars.2007.1556
64. Fukai T, Fukai M. Cross-talk between NADPH oxidase and mitochondria: role in ROS signaling and angiogenesis. *Cells*. 2020;9:1849. doi:10.3390/cells9081849
65. Zuo L, Fan Y, Wang F, Gu Q, Xu X. A SiRNA targeting vascular endothelial growth factor- A inhibiting experimental corneal neovascularization. *Curr Eye Res*. 2010;35:375–384. doi:10.3109/02713681003597230
66. Kvanta A, Sarman S, Fagerholm P, Seregard S, Steen B. Expression of matrix metalloproteinase-2 (MMP-2) and vascular endothelial growth factor (VEGF) in inflammation-associated corneal neovascularization. *Exp Eye Res*. 2000;70:419–428. doi:10.1006/exer.1999.0790